Comparison of GCM Column Shortwave Radiative Fluxes with Three-Dimensional Simulated Observations

W. O'Hirok and C. Gautier
Institute for Computational Earth Systems Science
University of California, Santa Barbara
Santa Barbara, California

Introduction

Comparisons are often conducted between global circulation model (GCM) outputs and satellite-derived measurements of cloud radiative forcing to access the model performance in simulating cloud-radiative processes. Differences that occur can be attributed to either a lack of understanding about the physical processes involved, parameterization of complex processes within general circulation models, or to difficulties in matching both the input and output of models with observations. Hence, in regard to the latter difficulty, comparisons between GCMs and observations necessitate both spatial and temporal averaging, which may mask the ability to understand the processes that account for the differences. To address this issue, we simulate observations with a three-dimensional (3-D) radiative transfer model, which avoids many of the parameterizations required for a GCM. By operating on the same input fields, comparisons between the simulated observations and the GCM output provide a means for discerning if discrepancies between actual observations and GCMs result from parameterization (e.g., plane-parallel assumption) or a missing physics.

Model Computations

Eight cloud fields with their accompanying atmospheric profiles were extracted from the NCAR (National Center for Atmospheric Research) Community Climate Model 3.0 (CCM3). The same atmospheric profiles, cloud liquid water amounts and cloud ice fractions are used in a 3-D Monte Carlo (MC) radiative transfer model. The cloud liquid water amounts are convolved with synthetic cloud fields to produce realistic clouds. While both models employ the same ice parameterizations, the primary differences between the 3-D and CCM3 models in the shortwave region are as follows:

- 3-D MC computations vs. single column delta-Eddington approximations.
- 751 wavebands in the MC vs. 18 spectral bands in the CCM3.
- Mie computations at 0.005 μm resolution for cloud liquid water microphysics in the MC vs. four spectral interval parameterizations in the CCM3.
- 3-D cloud distributions in the MC vs. plane-parallel in the CCM3.

Cloud Models

Cloud layers are derived from two-dimensional (2-D) images obtained from the National Aeronautics and Space Administration's (NASA's) moderate-resolution imaging spectroradiometer (MODIS) Airborne Simulator (MAS) (http://ltpwww.gsfc. nasa.gov/ MODIS/MAS/Home.html) and converted into 3-D distributions of liquid water using a multiplicative cascade approach. Rather than using a set of predefined weights to distribute the liquid water in the multiplicative process, the weights are derived directly from the cloud image. Two advantages of this approach are that the generated field represents a single realization of a cloud and not a statistical ensemble, and spatial coherence in the cloud field can be maintained by using weights that are derived locally.

Steps for cloud generation (Figures 1 and 2):

1. Cloud field is deconstructed in a reverse multiplicative manner.
2. Weights are computed by dividing each degradation by the following larger degradation.
3. Starting from smallest weight field (f256/f512), a set of four weights are extracted from location i, j on the horizontal plane.
4. These weights are randomly distributed among a cube located at i, j and k.

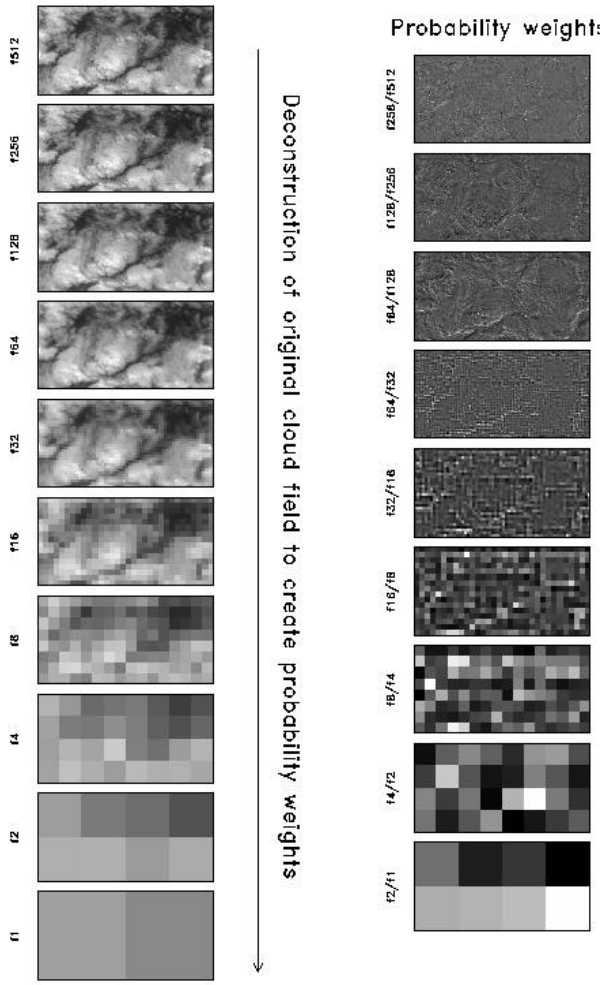

Figure 1. Deconstruction of MAS image to produce probability weights. Each image in left column represents a degradation of resolution by 2. Images in right column show division of degraded image by the subsequent degraded image.

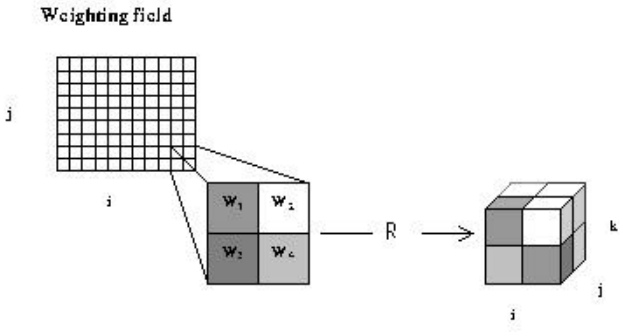

Figure 2. Schematic showing extraction of probability weights from field and random distribution among local cube.

5. This process is repeated for N additional cubes along the vertical axis at location i, j. N = H/L where L is the length of a pixel and H represents the maximum cloud thickness related to the atmospheric boundary conditions. Within the limits set by H, turbulence is assumed to be isotropic.

6. Once the process is completed at location i, j, new weights are derived at i+2, j and steps 3 through 6 are repeated.

7. Upon stepping through the entire field, a liquid water content (LWC) block, Q, is produced with cuboidal element dimensions of L.

8. At this point the next weight field is employed, L is doubled and LWC block Q_{+1} is produced.

9. When L=H, the process is stopped and the Q_s are multiplied together along with the non-randomized Q_s that had L>H to produce a single LWC block.

10. The LWC block is convolved with the profile of adiabatic liquid water and the vertical liquid water path at each pixel to produce cloud morphology.

11. Finally, specified bounded sets of effective radii (re) are allowed to vary spatially according to the LWC for each cuboidal.

Figure 3 shows a simulated stratus cloud type using this approach. This cloud layer along with a cirrus and convective cloud can be incorporated separately or in combination to produce a wide range of cloud field scenarios. In this study, the total LWC and cloud fraction are adjusted to equal the atmospheric conditions extracted from the CCM3 model run.

Results

Although eight cloud fields are compared in these study, only cases 1, 4, and 8 are displayed in Figure 4 and briefly discussed here. For each case, an image of vertically integrated optical thickness at 0.55μm; differences between 3-D and CCM3 computations of upwelling, downwelling and atmospheric column absorption; and differences in heating rate profiles are presented. The shaded bands represent the vertical extent of a cloud layer.

Case 1 represents an almost completely overcast stratus cloud. Because of the high solar zenith angle (70°) the stratus cloud appears optically thicker than the plane-parallel cloud of the CCM3 and produces more upwelling

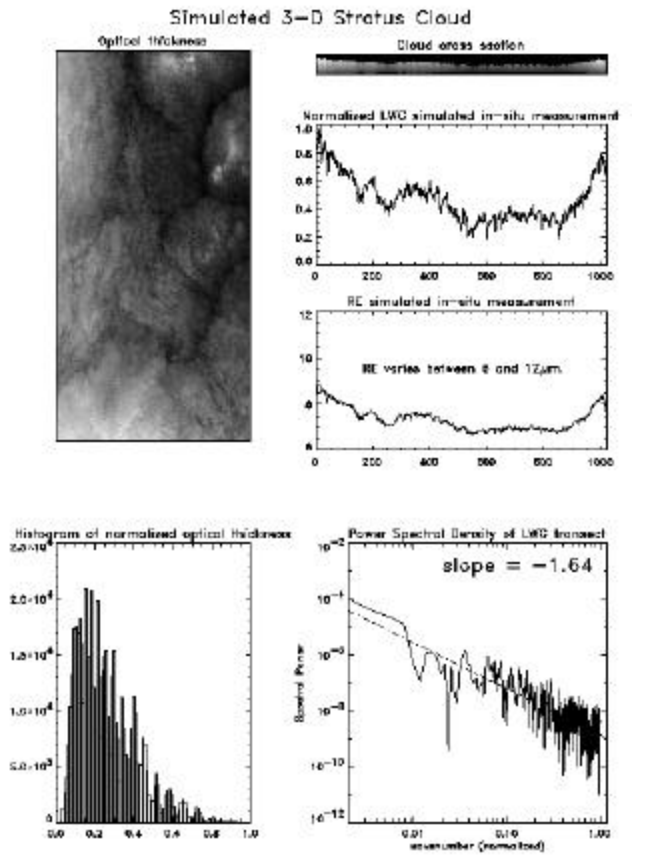

Figure 3. Simulated 3-D stratus cloud optical thickness variability image and cross-section, transects of normalized LWC and r_e, normalized optical thickness histogram and LWC power spectral density.

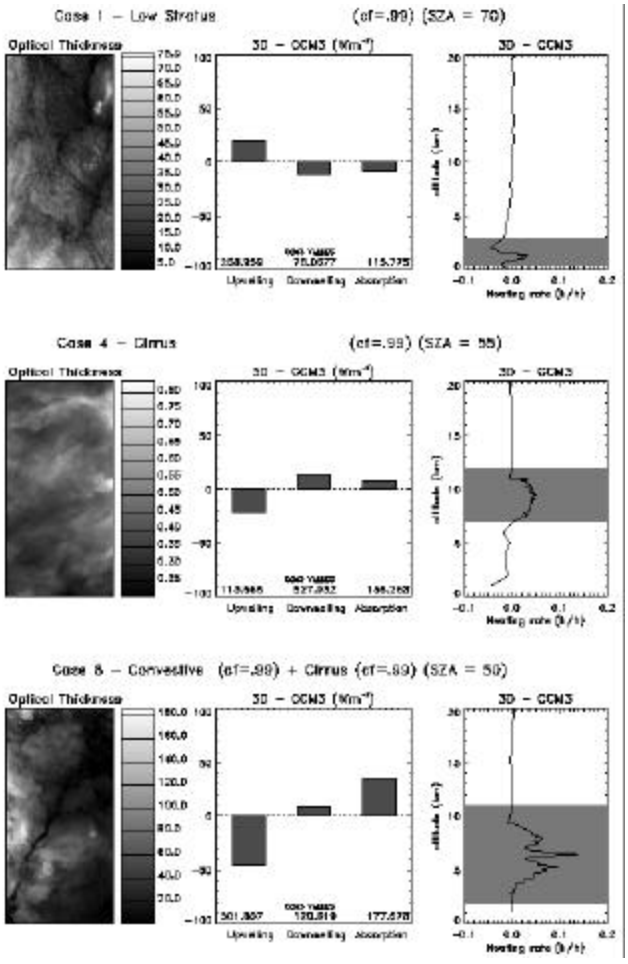

Figure 4. Vertically integrated optical thickness at 0.55 μm, differences between 3-D and CCM3 computations of upwelling, downwelling irradiance and atmospheric column absorption, and differences in heating rate profiles for cases 1, 4, and 8. The shaded bands represent the vertical extent of a cloud layer.

and lower downwelling flux. In turn, the reduced transmission below 1 km, where water vapor is at its densest, produces lower overall atmospheric absorption. The negative to positive change within the cloud for a difference between the 3-D and CCM3 heating rate is caused by the variability of the cloud top morphology of the 3-D cloud. For both clouds, the liquid water profile increases with height. However, the upper portions of the 3-D cloud are predominately clear and thus proportionally more liquid water occurs towards the base of the 3-D cloud compared to the CCM3 causing greater absorption by cloud droplets to occur there.

Case 4 represents a geometrically thick but optically thin cirrus cloud. Here, the 3-D computation produces less over all reflectance and greater transmission than the plane-parallel case of the CCM3. The result is caused by a combination of the sun being higher in the sky (55°) and a flatter cloud top that makes the nonlinear relationship between cloud reflectance and optical thickness dominate over cloud morphology effects. Absorption is slightly higher for the 3-D cloud throughout, as demonstrated in the heating rate profile.

Case 8 shows a cirrus cloud overlaying a convective cloud with altitude between 2 km and 11 km. Most notable in this case is the large reduction in upwelling flux caused by an increase of absorption by 35 Wm^{-2} for the 3-D cloud. This increase is mainly a function of photons entering the sidewalls of the convective cells and becoming trapped at mid-levels as evident by the spike of 0.15 K per hour in the solar heating rate.

Because the cloud fraction in these cases is 0.99, the greatest differences between the 3-D and CCM3 computations are related to the vertical distribution of cloud liquid water. For broken clouds, greater differences are expected to occur because the overlap between cloud layers can have many combinations. Additionally, for such cloud fields 3-D radioactive effects are at their strongest.

Acknowledgment

This research was supported by the U.S. Department of Energy Grants 90ER61062 and 90ER61986.